

A Bidirectional Deposition Model of Wax Crayons

Dave Rudolf
dave.rudolf@usask.ca

David Mould
mould@cs.usask.ca

Eric Neufeld
eric@cs.usask.ca

Department of Computer Science
University of Saskatchewan

Abstract

We present a physically-inspired model of wax crayons, which synthesizes drawings from collections of user-specified strokes. Paper is represented by a height-field texture, and a crayon is modelled with a 2D mask that evolves as it interacts with the paper. The amount of wax deposition is computed based on the crayon contact profile, contact force, and friction. Previously deposited wax is smeared by crayon action, based on wax softness and contact information. Deposited wax can also be carved from the paper by the crayon and redeposited at another location. The distributed wax is rendered using a simplified Kubelka-Monk model, which approximates light transmission and scattering effects.

Categories and Subject Descriptors (according to ACM CCS): I.3.3 [Computer Graphics]: Line and Curve Generation I.3.7 [Computer Graphics]: Three-Dimensional Graphics and Realism: Color, shading, shadowing, and texture

Keywords: nonphotorealistic rendering, procedural textures, interactive techniques

1. Introduction

Recent years have seen a proliferation of nonphotorealistic rendering styles, such as oil painting, pen-and-ink illustration, and copperplate engraving, among others. One thread of research has involved simulating specific traditional media, such as watercolours or pencils. In this paper, we describe a drawing primitive designed to mimic wax crayons.

Wax crayons possess certain characteristics that make them challenging to model. The crayon contact area is large enough that the paper cannot be treated as flat over the region of contact. The softness of wax is such that a substantial quantity of wax adheres to the page, and that previously deposited wax can be smeared and carved away by the action of later crayon strokes. However, wax is much more viscous than paints and inks, and so its interactions are different than these other media. Also, the crayon footprint can change shape over a short period of time, changing substantially even within a single stroke. Many different colours of wax crayon are commonly in use, and the interaction between multiple translucent materials offers a rendering challenge.

We present a method for simulating wax crayons based

on a physically-inspired model of wax deposition, smearing, and redeposition. Drawings are based on a collection of user-specified strokes; the effect at each point along a crayon's stroke is treated by first computing the crayon's contact profile, then depositing wax from the crayon to the paper, updating the crayon shape, smearing and possibly carving previously deposited wax. The final distribution of wax is rendered with a simplified Kubelka-Monk model, which accounts for light transmission and scattering through multiple layers of wax.

Wax crayons are archetypally associated with a certain highly simplified drawing style. Despite the occasionally onerous physical simulation we describe, we have endeavoured to retain a sense of fun in the project, and we hope that this carries through in the childish artistic style of the images we present.

2. Previous Work

Originally, nonphotorealistic rendering (NPR) branched from work in image processing and pattern recognition circles. The earliest work in NPR consisted of specialized dithering techniques [VdMG91, VB99]. Edge detection

and region extraction algorithms have been employed to decompose existing images or 3D models into their view-space elements: lines, curves, polygons, and the like [SS02, GG01]. The purpose of such work was to emphasize the important features of an object, and remove distracting details and imperfections. From these basic building blocks, another area of NPR research emerged: that which aims to simulate a particular artistic style or medium, as we do in this paper. Graphical primitives are interpreted as artistic strokes or patches made by the simulated artistic medium. Previous work simulated media such as pencil sketches [SS02, GG01] and drawings [LMHB00, MG02b, TNF99], charcoal drawings [MG02a], watercolour [CAS*97], and stained glass [Mou03]. Also, some work tries to simulate particular artistic styles, such as those of Dr. Seuss and Geoffrey Hayes [KMN*99].

Existing nonphotorealistic rendering methods follow distinct branches. One such branch makes use of the aforementioned image processing techniques to extract primitives from 2D images and related data, such as depth buffers and stencil masks [SS02, TC00]. Alternatively, 3D geometry can be used directly [MG02b, GG01, MG02a, KMN*99]. Lastly, interactive systems have been developed that depend on user-defined input [KMM*02, CAS*97]. Our work falls into this last category, although we have designed our model to be independent of the source of input.

Techniques to represent artistic media vary widely, depending on the media being represented. A physically-based representation of paper has been developed [TNF99], but 2D height maps are widely used to represent the high-level texture of paper. Since a crayon's contact surface is relatively large, we also represent paper with height maps. With this approach, numerous texture synthesis methods have been employed to create visually appealing height maps [CAS*97, Per85, vW91]. We also make use of these methods.

In modelling actual artistic implements such as brushes and pencils, it is common practice to use a static one-dimensional height mask to represent a cross-section of the implement perpendicular to the stroke path [SS02, GG01]. This simple representation limits the types of interaction that can be modelled. Some work uses texture mapping to simulate artistic media in an abstract sense [LMHB00, MG02a]. These methods assume that paper is relatively predictable in structure. Other research makes use of 2D masks to represent an implement [CAS*97, KMM*02, Ado99]. These models typically assume that the mask, once initialized, is static throughout its lifetime. Sousa and Buchanan [SB99] modelled graphite pencils using a polygon to represent the pencil tip. In their system, each vertex of the polygon is modified throughout the length of each stroke. Their method was used to represent a pencil that could rotate and pivot, and also have nonuniform pressure distributions. Points within

the polygon must be interpolated from the surrounding vertices, so there is a limit to the kinds of profiles that can be represented. The most dynamic model of an artistic tool thus far was developed by Baxter et al. [BSLM01]. Baxter's work makes use of polygon meshes to represent different styles of artistic brushes. These meshes deform as the brush comes into contact with paper, accounting for spring tension in the bristles.

Finally, some methods require an explicit rendering step to generate the final image. A great deal of research has been dedicated to volumetric rendering techniques [LL94] and light scattering [JMLH01]. Takagi et al. [TNF99] used such methods to render their model of coloured pencils. A volumetric approach is the most flexible, allowing arbitrary views of the modelled medium. However, such an approach is also very costly, especially for large number of pigment layers. A convenient compromise is the Kubelka-Monk colour model, which has been used to approximate the optical properties of translucent pigments [HM92]. This colour model assumes that the viewing angle is normal to the paper.

A deficiency of many current NPR techniques is that they model some amount of simple pigment deposition, apply the results to an incrementally developed image, and then start the next phase of deposition with an empty pigment model [KMM*02, CAS*97, SS02, GG01]. This eliminates the possibility of interaction between deposition phases. Sousa and Buchanan [SB99] have successfully modelled smudging of graphite pencil, but consider only a single pigment colour. Baxter et al. [BSLM01] also allowed for some level of smearing. Existing pigment is either considered to be "wet" and will interact with the brush, or the pigment is "dry" and will not be considered for interaction.

Previous attempts have been made to generate crayon-like images. Adobe Systems® has included a conté crayon filter with their distributions of Photoshop® for some time [Ado99]. This filter is simply a textured dither, and does not capture the true nature of wax. Kalnins et al. [KMM*02] have used brush masks in a stroke-based system to deposit wax onto a paper model, but they do not account for interaction between layers of wax. Thus far, Corel Corporation's Painter™ 8 [Cor03] package has the most rigorous model of crayons. This system does model wax interaction, similar to the work of Baxter et al. [BSLM01]. Corel's model has two noticeable deficiencies. First, the colour model used is a purely subtractive model. That is, it does not consider the light-scattering effect that is seen in real wax. When different colours of wax are blended, they do not appear as real wax does. Second, the wax deposited by each stroke is immediately mixed with any previously deposited stroke, and the brush absorbs the resulting colour. This would never occur with real crayons because of the high viscosity of wax. Typically, only the top layer of deposited wax will interact with the crayon. In this paper, we strive to eliminate the afore-

mentioned discrepancies between real crayon drawings and simulated ones.

3. Modelling Wax

We are concerned with how a crayon leaves its trail of wax as it passes across the surface of paper. Many physical processes affect the crayon. We forego a rigid physical model, and concentrate on the more prominent natural effects; our representation of wax is based on observation. To understand the medium, we studied wax deposition using microscopy at different levels of magnification. Since wax has a high viscosity, our observations were done at relatively low magnification levels: between $6\times$ and $75\times$ zoom.

In this section, we present the basic components of our wax model. In particular, we discuss our representations of wax crayons and paper, as well as our process for generating paper texture. We then introduce the algorithm that describes the interaction between a crayon and a paper texture. This algorithm first determines the crayon’s vertical position with respect to the underlying paper and a scalar force. The crayon’s location is then used to smear and carve wax that was previously deposited onto the paper, and also to deposit new wax. Lastly, we render the model using the Kubelka-Monk method.

3.1. Representation of Media

We follow traditional methods of representing paper as a 2D height map [SS02, CAS*97]. Like recent work in NPR [SB99, BSLM01, TNF99], our system must retain a record of deposited material throughout the evolution of the image. Because wax is easily smeared and carved, we must keep a dynamic model of wax as it adheres to a static paper texture.

To do so, we maintain a column of wax layers at each cell of the paper texture. The columns are normal to the gross plane of the paper. Each layer has its own *height*, *colour*, *light transmittance*, and *scattering* properties, which are used in our rendering algorithm (see section 4). For efficiency, adjacent wax layers with the same properties are merged together. Also, sufficiently thin layers are blended with adjacent layers. Layer blending helps prevent the proliferation of extremely thin layers, mostly caused by wax smearing and redeposition (see sections 3.6 and 3.7).

The actual crayon is modelled in a similar fashion. The profile of the crayon is also modelled as a 2D height map, where height values represent the crayon’s distance from the gross plane of the paper. Each cell in the crayon’s mask initially contains wax with the same colour, transmittance, and scattering properties. The height values in the 2D mask are modified as the crayon is worn down by friction.

Our dynamic mask allows us to model a variety of profiles that real crayons would have. Using this method, we

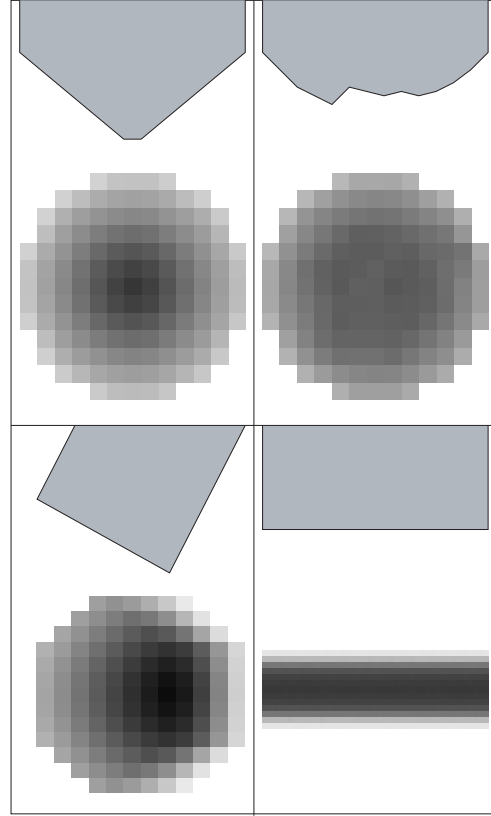


Figure 1: Example height profiles of crayons. Each of the four images has a longitudinal views of a hypothetical crayon shape at the top, and the crayon mask that represents the shape at the bottom. The height of the masks’s cells are depicted by their intensity. The top-left image is a sharpened conic crayon, the top right is the same crayon after abrasion, the bottom left is the flat back end of a crayon and the bottom right is the long side of a crayon.

can represent a variety of crayon tips. As seen in Fig. 1, the mask can represent a tip that is initially sharpened into a cone shape. Throughout a drawing stroke, the mask can be modified to simulate the crayon tip as it is progressively abraded into a blunt shape. Sharp features of the paper texture may even carve minor ridges and hollows into the tip of the crayon. The crayon’s profile can also be tailored to represent the sharpened back-end rim, or even the long side of the crayon itself. Although the height map representation does prevent us from modelling some possible wax configurations (mainly, vertical concavities caused by extreme abrasion and adhesion), it is sufficient for modelling interactions with widely-used media, such as paper, which are relatively flat.

Each cell in the crayon mask also has an *area* property associated with it. This is done to counteract aliasing artifacts

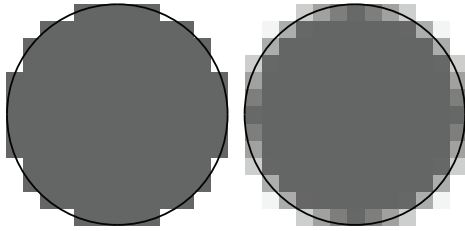


Figure 2: Example area profiles of crayons. The intensity of each crayon cell is inversely proportional to that cell’s assigned area. On the left is an aliased crayon mask, and on the right is an anti-aliased mask. The true area of the crayon is shown in dark black on top of each mask.

that were observed in our initial crayon renditions. Specifically, spurious stepping effects appeared when a stroke’s direction was at a small angle (less than 20°) from the Cartesian axes. Fig. 2 shows examples of area profiles for round crayons.

As with the height field used to represent paper texture, the cells in the crayon mask can have layers of wax added to them. This is done to mimic the way that loose flakes of wax are pressed against real crayons and carried to other locations of the paper.

3.2. Generation of Paper Texture

When generating final images of crayon drawings, paper texture is an important consideration. Although our deposition, smearing, and redeposition methods do not require any particular texture, they do depend on the texture. Real paper textures vary widely. Ideally, we should choose a texture that approximates a kind of paper that is typically associated with wax crayons. In consequence, we have striven to find a height field texture which is quite rough, akin to an inexpensive construction paper that is commonly used by children.

We used the lunar texture postulated by van Wijk [vW91], which has a suitable combination of roughness and coherence. Our version of this texture was generated by convolving a quarter-circle arc with a lattice populated by uniform noise. The convolution mask is shown in Fig. 3 and an example of the texture thus derived is shown in Fig. 4.

Our deposition and smearing algorithms (see section 3.3) require that some texture be provided, but make no assumptions about the nature of that texture. To test this aspect of our model, we have also generated textures that are fundamentally different than the aforementioned lunar texture. For example, we created a stippled texture by using a 2D mask to scale the amplitude of uniform noise. This mask is tiled across the noise lattice to impose a repetitive structure upon the generated texture. An example of one such texture is seen

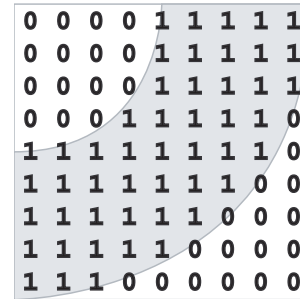


Figure 3: Convolution mask used to generate van Wijk’s lunar texture.

in Fig. 4. Also shown in Fig. 4 is a texture that was photographically acquired from real construction paper. For this texture, intensity values of the acquired image were used as the height values of the texture. Of course, the intensities of construction paper may not be accurate measures of the construction paper’s height profile. The acquired texture is shown merely as another example of our model’s robustness.

3.3. High-Level Interaction Algorithm

Our model of crayons mimics the dominant interactions that are observed between real crayons and paper. First, we note that wax is deposited by the crayon. The volume of deposited wax depends on the size of the contact area between the crayon and paper, the slope of the paper over that area, and the force that is exerted by the crayon onto the paper. Second, wax that has been deposited onto the paper can be smeared around when the crayon passes over it. The smearing process pushes wax from the peaks of the paper texture, and down into adjacent lower regions. Smearing also has a directional component, in that the crayon will push wax in its directional heading. In this manner, wax can be pushed over ridges in the paper. Fig. 5 illustrates the interactions of a crayon with the paper texture.

The flow of wax between a crayon and paper is bidirectional. A crayon deposits wax onto the paper, but it can also lift deposited wax from the paper. The crayon may then transport the annexed wax and redeposit it at a different location. This process of redeposition is described in section 3.7.

When creating wax renditions, we use lines and curves as our drawing primitive. Although artists who work with acrylic crayons have other techniques at their disposal such as dabbing, children typically use crayons for line drawings. Our method only requires that the directional heading of the crayon be known at each step in the simulation. As such, our model can support curved arcs such as splines.

To simulate a crayon stroke, we consider the endpoints P_1 and P_2 , the crayon’s height mask M , the scalar force f applied by the crayon to the paper, and the set C of colour properties of the wax. For any given crayon position, we must



Figure 4: Wax deposition with different paper textures: (top) lunar convolution, (center) stipple restriction, and (bottom) real construction paper acquired at 800dpi.

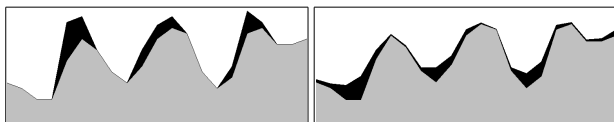


Figure 5: Hypothetical interaction between crayon and paper: (left) Wax deposition, (right) Smearing.

prepare the crayon, and modify the wax model. First, we adjust the crayon height values with respect to the applied force, the crayon's height profile, and the profile of the paper (and the wax deposited on it) at the current location. We then use the new height values to modify the set of wax layers L that lie on the paper. In modifying these layers, we first determine the amount of previously deposited wax that can be annexed by the crayon from the paper. The wax that remains on the paper is then considered for smearing. Lastly, the crayon deposits new wax onto the paper, some of which is wax that was carved off of the paper in an earlier time step. This process is summarized in Fig. 6.

```

proc drawLine(  $P_1, P_2, M, C, f, L$  )
  for each point  $P_i$  on the line segment  $\vec{P_1P_2}$ 
    adjustCrayonHeight(  $P_i, M, f, L$  )
    reclaimWax(  $P_i, \vec{P_1P_2}, M, L, f$  )
    smearExistingWax(  $P_i, \vec{P_1P_2}, M, L$  )
    addNewWax(  $P_i, \vec{P_1P_2}, f, M, C, L$  )
  end
end

```

Figure 6: Summary of the actions taken when a line is drawn.

Of course, to draw a line, we only choose points P_i that are appropriate for the resolution of our paper texture. In the following sections, we give detailed algorithms for each of procedures in Fig. 6.

3.4. Crayon Compression Due To Force

When drawing a line with a crayon, we must remove some volume of wax from the crayon and deposit it onto the paper underneath. The volume of deposited wax depends on the values of the crayon's height mask, relative to the local height of the paper. The simulation of all interactions between a crayon and paper are dependent on the vertical position of the crayon.

Since the crayon's cells will potentially be worn away with each movement, we must adjust the crayon's overall height at each step so that, at the next step, the crayon is exerting the same amount of force upon the paper. To do so, we assume that the wax compresses linearly, and use Hooke's Law of Compression to numerically determine the appropriate vertical displacement.

Hooke's Law [CJ95] can be written

$$F = Y \frac{\Delta L}{L_0} A, \quad (1)$$

where Y is Young's modulus constant, ΔL is the amount of compression, L_0 is the unstressed length, and A is the cross-sectional area. If we assume that the length of the crayon L_0 is approximately constant, being much greater than the

change in length ΔL , then we can reduce the above equation to:

$$F = \lambda A \Delta L. \quad (2)$$

For the constant λ , we simply choose a value that produces aesthetically pleasing results.

We can sum up the force contributed by each crayon cell onto its corresponding paper cell, setting the contribution to zero if the crayon cell is above its paper cell. This latter step prevents us from calculating the crayon's displacement directly. We no longer have a continuous function to evaluate, as the force is described by a piece-wise linear function. Instead, we use Newton's method to find a displacement that gives us the desired amount of force, within some tolerance ϵ . This tolerance can be chosen to suit the precision of the implementation, so that refinement stops when round-off error is greater than the range of possible values. However, the cost of simulation is dramatically reduced when a suitable tolerance is imposed, with negligible visual difference in the resulting image. The error threshold that we have chosen to use is given in Table 1, along with other parameters of our model.

To determine the vertical displacement of the crayon, we consider the height of the crayon $h_{m_{ij}}$ at each mask cell m_{ij} , and the height of the paper $h_{P_{ij}}$ and also of all the wax layers $h_{L_{P_{ij}}}$ at the corresponding location P_{ij} . The crayon height calculation is summarized in Fig. 7. As seen in Fig. 8, the amount of deposited wax varies with the applied force.

3.5. Frictional Deposition

Friction is the process by which wax is broken from the crayon and deposited onto the paper. We model friction on two levels, macroscopic and microscopic. On a macroscopic level, we are concerned with the force of the crayon normal to the surface of the paper. As the crayon encounters convex features in the paper's texture, it leaves behind some quantity of wax. On a microscopic level, we use a coefficient of friction to approximate the roughness of the paper on a smaller scale. The amount of deposited wax should be proportional to the frictional force, which is defined as:

$$\vec{F}_F = \mu \vec{F}_N = \mu \vec{N} \frac{\vec{N} \cdot \vec{F}_C}{\|\vec{N}\| \|\vec{F}_C\|} \quad (3)$$

where

\vec{F}_C is the force of the crayon on the feature's surface,

\vec{F}_F is the force of friction,

\vec{F}_N is the crayon force normal to the feature's surface,

\vec{N} is the surface normal of the feature, and

μ is the coefficient of friction for the paper.

With our height-mapped paper texture, we interpolate adjacent height values to define a plane against which the

```

proc adjustCrayonHeight(  $P, M, f, L$  )
   $h_{min}^{crayon} \leftarrow \min(\forall h_{m_{ij}} : m_{ij} \in M)$ 
   $h_{min} \leftarrow \min(\forall h_{P_{ij}} : m_{ij} \in M \text{ and } P_{ij} = P + (i, j))$ 
   $h_{max} \leftarrow \max(\forall h_{P_{ij}} : m_{ij} \in M \text{ and } P_{ij} = P + (i, j))$ 
  while  $h_{max} - h_{min} > \Delta$ 
     $h_{mid} \leftarrow (h_{max} + h_{min}) / 2$ 
     $f_{h_{mid}} \leftarrow 0$ 
    for each  $m_{ij} \in M$ 
       $\delta h = h_{P_{ij}} + h_{L_{P_{ij}}} - (h_{m_{ij}} - h_{min}^{crayon} + h_{mid})$ 
      if  $\delta h > 0$ 
         $f_{h_{mid}} \leftarrow f_{h_{mid}} + \lambda \delta h$ 
      end
    end
    if  $f < f_{h_{mid}}$ 
       $h_{min} \leftarrow h_{mid}$ 
    else
       $h_{max} \leftarrow h_{mid}$ 
    end
     $h_{mid} \leftarrow (h_{max} + h_{min}) / 2$ 
  for each  $h_{m_{ij}}$ 
     $h_{m_{ij}} \leftarrow h_{m_{ij}} - h_{min}^{crayon} + h_{mid}$ 
  end
end

```

Figure 7: Calculation of the crayon height values.

crayon is moving, and calculate friction. This friction is determined with respect to that plane, the given scalar force being applied to the paper by the crayon, and the directional heading of the crayon itself (i.e., the direction of the stroke being drawn).

The value of μ depends on whether the crayon is interacting with clean paper or with paper that already has some wax. To add to the complications, a region of paper with an extremely thin layer of wax will have different frictional properties than a region with a thicker layer of wax. Current literature on the production of pulp and paper has little to suggest an appropriate coefficient for paper alone. While tribology does offer insight into the wear properties of polymers and resins [BG91, Pla95], it is difficult to determine the ratios of esters, fatty acids, alcohols and hydrocarbons present in wax crayons. Since our model is not rigorously analytical, we artistically choose the two friction coefficients, and smooth the transition between them for thin layers of wax.

To deposit wax, we consider the point P at which the crayon is located, the crayon's directional heading \vec{V} , the crayon's height mask M , the set of colour properties C of the crayon, and scalar force f which is normal to the gross plane of the paper. The wax deposited at each point P_{ij} is added to the set of layers $L_{P_{ij}}$ at that point. An example of wax deposition using our model is shown in Fig. 12. The method for computing deposition appears in Fig. 9.

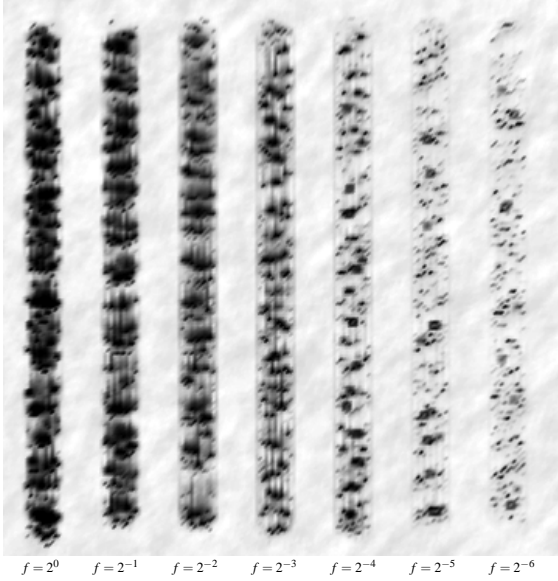


Figure 8: Wax deposition with different amounts of force.

```

proc addNewWax(  $P, \vec{V}, M, C, f, L$  )
   $\vec{V} \leftarrow \vec{V} / \max(x_{\vec{V}}, y_{\vec{V}})$ 
  for each  $m_{ij} \in M$ 
     $P_{ij} \leftarrow P + (i, j)$ 
     $P'_{ij} \leftarrow P_{ij} + \vec{V}$ 
     $\vec{S}_{ij} \leftarrow (x_{\vec{V}}, y_{\vec{V}}, h_{P'_{ij}} - h_{P_{ij}})$ 
     $\vec{F}_{ij} \leftarrow (x_{\vec{V}}, y_{\vec{V}}, -f)$ 
     $\alpha \leftarrow 1 / (1 + h_{P'_{ij}}^{wax})$ 
     $\mu_{ij} \leftarrow \alpha \mu_{paper} + (1 - \alpha) \mu_{wax}$ 
     $\delta h_{P'_{ij}}^{wax} \leftarrow \mu (h_{P'_{ij}} - h_{m_{ij}}) \sin(\vec{S}_{ij}, \vec{F}_{ij})$ 
     $h_{m_{ij}} \leftarrow h_{m_{ij}} + \delta h_{P'_{ij}}^{wax}$ 
     $L_{P_{ij}} = L_{P_{ij}} + \{(\delta h_{P'_{ij}}^{wax}, C)\}$ 
  end
end

```

Figure 9: The method for moving wax from the crayon to the paper.

In our algorithm, we compute several intermediate results. First, we find the point P'_{ij} that is along the crayon's heading and is closest to one of the eight neighbours. We use P'_{ij} to find the upcoming slope vector \vec{S}_{ij} of the paper along the path of the crayon. We also determine the force vector \vec{F}_{ij} and a coefficient of friction μ_{ij} given the amount of previously deposited wax.

3.6. Smearing

Smearing is a characteristic of the medium of wax, in the same way that bleeding is a characteristic of watercolours. As a crayon moves across paper, it smears the wax into adjacent regions. Both newly and previously deposited wax are smeared. To simulate smearing, we employ a smearing mask that encompasses the current paper cell and its eight neighbours. Each value in the mask determines the proportion of wax that is to be moved from the centre cell to the cell underneath the given mask location. This smearing mechanism only considers the effects of a single grid cell and its eight neighbours. Because of the viscosity of wax, we assume that the vast majority of the involved pressure is absorbed by the immediate neighbours. Such an assumption would not hold for pastels or softer media. With real pastels, pressure would be propagated a greater distance.

To generate the smearing mask, we consider the relative location of each value (x, y) , the height of the paper (and its wax) Δz at that location, and the directional heading \vec{V} of the crayon. Mask elements are given by the following equation:

$$S_{xy} = \frac{1}{\|(x, y)\|} \left(\alpha \Delta z + \beta (x, y) \cdot \hat{V} \right). \quad (4)$$

We set the center mask value $S_{0,0}$ to zero, so that we avoid “smearing” wax back onto itself.

```

proc smearExistingWax(  $P, \vec{V}, M, L$  )
  for each  $m_{ij} \in M$ 
     $S$  is a  $3 \times 3$  matrix.
    for each  $s_{qr} \in S$ 
       $s_d \leftarrow \max\{0, \hat{V} \cdot (\hat{q}, r)^\perp\}$ 
       $s_f \leftarrow (h_{P_{ij}} + h_{L_{P_{ij}}}) - (h_{P_{(i+q)(j+r)}} + h_{L_{P_{(i+q)(j+r)}}})$ 
       $s_{qr} \leftarrow \alpha s_f + \beta s_d$ 
    end
     $S \leftarrow vS / (\sum s_{qr})$ 
     $\delta h_{wax} \leftarrow h_{L_{ij}} (h_{L_{P_{ij}}} + h_{P_{ij}} - m_{ij})$ 
     $L_{P_{ij}'} \leftarrow \{l_a, \dots, l_n\} : \sum h_{l_i} = \delta h_{wax}$ 
    for each  $s_{qr} \in S$ 
      for each  $l_k \in \delta L_{P_{ij}'}$ 
         $L_{(i+q)(j+r)} \leftarrow L_{(i+q)(j+r)} + s_{qr} l_k$ 
      end
    end
  end
end

```

Figure 10: Pseudocode for the smearing algorithm.

In the above algorithm, we determine smearing factors to represent the relative portions of deposited wax that smeared as a result of fluidic flow (s_f) and directional pulling (s_d). The values of α and β can be chosen to match a particular smear pattern, or can be proportional to the crayon's scalar velocity. Once the mask is constructed, it is normalized to a wax viscosity factor v . The wax layers are then

removed from the current paper cell, and distributed to the eight neighbors according to their mask values. Smearing is summarized in Fig. 10. Some results from our smearing algorithm are shown in Fig. 12.

3.7. Redeposition

One of the properties of wax is that it is self-adhesive. As a crayon moves across the paper, it will carve out wax that has already been deposited on the paper. The resulting loose volume of wax may then be pressed against the crayon, where it will be carried along to be deposited again to a different region of the paper. The effect of this redeposition process is quite evident in real crayons. Strokes that move over existing wax tend to show light streaks of the original wax pigments. We account for wax redeposition in a manner similar to the bidirectional deposition used by Baxter et al. [BSLM01] for paint pigments. In the Baxter model, a brush’s pigment colour is blended with pigments that are on the canvas. This blending occurs for each time step of the simulation. As the brush moves across the canvas, the presence of the brush’s original colour will decay exponentially until the brush contains only pigments that it has absorbed from the canvas.

Because of the high viscosity of wax, the pigments in our system do not mix in the same manner as paints. Instead, layers of wax are removed from the paper and placed back onto the crayon. In this way, the reclaimed wax will be redeposited in a linear fashion, rather than exponential. Also, paint on a canvas will begin mixing with a brush’s pigment as soon as the brush comes into contact with the canvas. However, no significant volume of deposited crayon wax will stick to the crayon on mere contact. The crayon must carve the wax off of the paper. Thus, the reclaimed wax accumulates in front of convex features of the crayon, relative to the stroke direction. To simulate the directional nature of wax reclamation, we first determine the amount of wax to be reclaimed by the crayon from the paper. We then use a mask S that encompasses the current crayon cell and its eight neighbours, similar to the smearing mask described in section 3.6. This mask stores the cosine of the angle between each of its cell positions and the directional heading of the crayon. Fig. 11 shows the details of our wax reclaiming method. Note that the distribution mask S depends only on the heading of the crayon \vec{V} , the scalar force f , and an artistically chosen reclamation factor γ . Thus, S can be precomputed at the start of each linear crayon stroke. The effects of our redeposition method can be seen in Fig. 12.

3.8. Parameters of the Model

Although we have not attempted to construct a thorough physical simulation of wax, our model is quite flexible. Various parameters in our system can be adjusted to represent other artistic media. Table 1 summarizes these parameters and gives the values we used.

```

proc reclaimWax(  $P, \vec{V}, M, L, f$  )
  for each  $m_{ij} \in M$ 
     $S$  is a  $3 \times 3$  matrix.
    for each  $s_{qr} \in S$ 
       $s_{qr} \leftarrow \max\{0, \hat{V} \cdot (\hat{q}, r)\}$ 
    end
     $S \leftarrow \gamma f S / (\sum s_{qr})$ 
     $\delta h_{wax} \leftarrow \max\{0, h_{m_{(i+q)(j+r)}} - h_{m_{ij}}\}$ 
     $L_{pij'} \leftarrow \{l_a, \dots, l_n\} : \sum h_{l_i} \leq \delta h_{wax}$ 
     $L_{pij} \leftarrow L_{pij} - L_{pij'}$ 
    for each  $s_{qr} \in S$ 
      for each  $l_k \in \delta L_{pij'}$ 
         $m_{(i+q)(j+r)} \leftarrow m_{(i+q)(j+r)} + s_{qr} l_k$ 
      end
    end
  end

```

Figure 11: Algorithm for reclaiming deposited wax.

Symbol	Description	Value
μ_{wax}	Frictional coefficient of wax.	0.5
μ_{paper}	Frictional coefficient of paper.	2
ν	Viscosity of wax.	0.5
α	Flow smear factor.	0.2
β	Directional smear factor.	$1 - \alpha$
γ	Wax Reclamation factor.	0.35
λ	Wax compression resistance factor.	0.0005
ϵ	Force accuracy factor.	$\lambda/4$

Table 1: Parameters of our model.

4. Rendering

We next turn our attention to generating images from the wax model. Wax is best treated as a translucent pigment, so simple additive and subtractive colour models such as RGB and CMY are inadequate. Instead, we employ a simplified Kubelka-Monk (KM) model [HM92]. The KM model approximates spectral *transmittance*, *scattering*, and *interference*. The value of these properties can be inferred by two specified colours [CAS*97]. Each of these colours is the observed result of a layer of pigment overtop of uniform background: one is the result with a black background, and the other with a white background. From these two resulting colours, KM theory provides a means of interpolating the colour that results from an arbitrarily thick layer of pigment with any given background. The KM model does so by in-

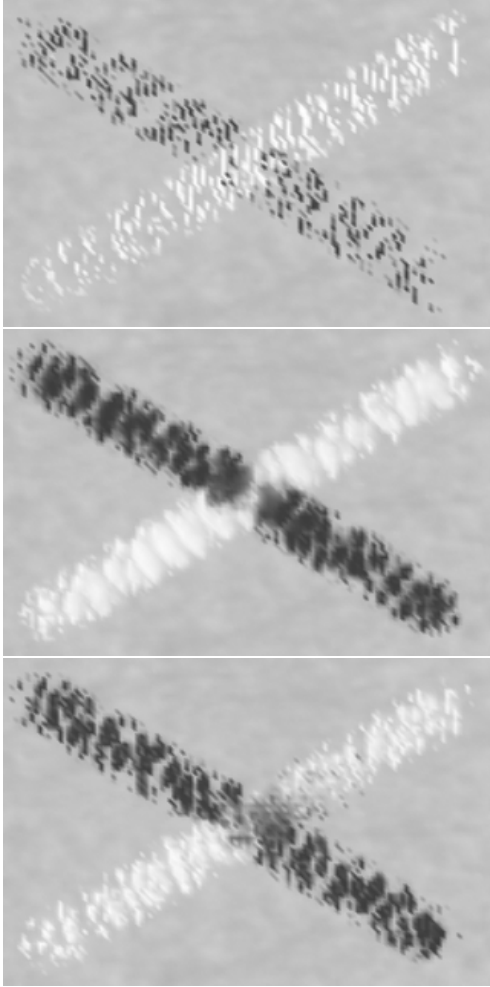


Figure 12: Modelled interaction between crayon and paper: (top) Wax deposition, (center) Smearing, (bottom) Redeposition. All images consist of a stroke of a dark coloured wax, followed by a stroke of a light coloured.

ferring how much light is scattered by the pigment medium, and how much is transmitted through the medium. The KM model also approximates changes in hue due to thin-film interference.

In our model, we ignore interference effects, as we did not observe them to contribute significantly to real crayon drawings. Consequently, each crayon is associated with a single RGB colour property, as well as *transmittance* and *scattering* factors. These factors apply equally to all three colour channels.

As mentioned previously, extremely thin layers of wax are merged together. The optical properties of the resulting layer are set to weighted averages of the two layers that were merged. Each layer's contribution to the resulting blended

layer is proportional to its height. This is a gross simplification of the KM model, but still produces acceptable results and significantly decreases the computational cost of the smearing algorithm.

To render the wax model, we consider the colour of the paper texture $C_{P_{ij}}$ at each point P_{ij} on the paper. To calculate the colour that results from a layer of wax $l_k \in L_{P_{ij}}$, we make use of the layer's colour C_{l_k} , its transmittance t_{l_k} , and its reflectance r_{l_k} . Details of the calculation are given in Fig. 13.

```

proc render(  $T$  )
  for each point  $P_{ij}$  on the paper texture  $T$ 
    Colour  $C_{ij} \leftarrow C_{P_{ij}}$ 
    for each wax layer  $l_k$  at point  $P_{ij}$ 
       $C_{ij}^{transmit} \leftarrow (t_{l_k} C_{l_k})^{h_{l_k}} C_{ij}$ 
       $C_{ij}^{scatter} \leftarrow 1 - (1 - C_{l_k})^{r_{l_k} h_{l_k}}$ 
       $C_{ij} \leftarrow C_{ij}^{transmit} + C_{ij}^{scatter}$ 
    end
  end
end

```

Figure 13: Our simplified Kubelka-Monk rendering algorithm.

We have endeavored to duplicate the optical properties of common children's crayons. Fig. 14 illustrates the optical properties of our generated crayons, as compared to real wax crayons. Table 2 lists the crayons we simulated and their empirically determined properties.

5. Results

Fig. 15 shows examples of final images. In the first image, interaction between colours is visible, particularly at the edges of the man's tie. We can also see the effects of differing friction on the man's shirt: the periwinkle crayon was applied first, and when the sea-green crayon was used it preferentially deposited wax in regions which had been bare. Interaction between colours is also apparent in the second image, particularly in the red and yellow portions of the character's hair, and on the polkadots of the pajamas. This image also demonstrates the scattering component of our KM model: the crayons' colours are visible even when the background is black. Fig. 16 has more examples of drawings that were generated by our methods.

Although efficiency was not our primary concern, we did not want to impose long rendering times on the user. Our implementation is not efficient enough for use in a real-time rendering pipeline. It is suitable for interactive stroke-based applications, provided that the user has a high-end workstation. Depending on line length, crayon contact area, and amount of force, processing each crayon stroke requires between 0.1 and four seconds on a 2.4GHz Pentium 4. Rendering the image can also take up to a second for a 500x500



Figure 14: Appearance of (top) real wax crayons, and (bottom) our generated crayons.

Crayon	Colour	R	G	B	T	S
	red	0.95	0.45	0.45	0.605	0.0425
	orange	0.999	0.55	0.3	0.77	0.03
	yellow	0.95	0.9	0.2	0.869	0.0425
	green	0.35	0.8	0.35	0.55	0.06
	blue	0.3	0.5	0.9	0.77	0.045
	purple	0.65	0.45	0.75	0.715	0.05
	brown	0.8	0.6	0.55	0.495	0.075
	black	0.26	0.25	0.245	0.935	0.05
	grey	0.42	0.4	0.39	0.594	0.275
	white	0.8	0.8	0.78	0.88	0.175
	periwinkle	0.7	0.7	0.9	0.605	0.125
	sea green	0.6	0.9	0.65	0.55	0.1
	orchid	0.85	0.4	0.84	0.88	0.075

Table 2: Optical properties of simulated crayons.

canvas image full of multiple wax layers. Memory can also become a concern. In our implementation, each pixel can require on the order of hundreds of bytes, depending on the number of wax layers that reside at the pixel. The memory footprint of the system can be reduced by allowing more of the thin wax layers to be merged, as mentioned in section 3.1.

For conventional home PCs, our model could be used for an effective preview-and-render system. The most time con-



Figure 15: Sets of user-defined strokes (left) and the resulting crayon rendering (right) generated by our methods. The bottom set of images also show an outline drawing from a colouring book that was used to create the image. This outline is rendered in the background of all wax layers for the resulting image.

suming parts of our system are the smearing and redeposition algorithms. Although smearing is quite essential to the end result of an image, the redeposition effect is arguably less important. It could be omitted during periods of user interaction, and then introduced in a final simulation stage in which the drawings strokes are processed again from memory. One could also reduce the requirements of our system by simply decreasing the resolution of the preview image, and scale the crayon mask's size and the stroke coordinates accordingly. This will still include both smearing and redeposition effects, but may not give a good estimate of the final image. Perhaps a better way to increase efficiency in both CPU time and memory usage is to increase the threshold that controls the maximum height of wax layers that are allowed to blend with adjacent layers in the same column.



Figure 16: Sample images generated with our wax deposition model.

As the blending threshold increases, our redeposition algorithm becomes similar in nature to that of the work of Baxter et al. [BSLM01].

6. Conclusions and Future Work

We presented a physically inspired model of wax crayons that extends previous work by representing crayons as dynamic 2D height masks. This approach allows us to more accurately model crayon wear as it interacts with paper, and to represent different configurations of crayons: sharpened, blunt, turned on its side, etc.

Images are generated with user-defined strokes as primitives. Each stroke deposits wax on the paper, and at each point we also model the crayon's interaction with previously deposited wax. The final distribution of wax is rendered using the Kubelka-Monk colour model, treating the wax as a collection of plane parallel layers.

We show some images generated by the model, revealing both strengths and weaknesses. Overall, the images resemble crayon drawings. The erratic placement of wax within the bounds of a stroke is captured. However, some observed phenomena are not captured by the model. First, and most prevalent, real wax does not wear as discretely as we have modelled it. Wax is a self-adhesive substance, and so when it is removed from one region of a crayon's tip, it may bring along wax from adjacent regions.

Although our model is not presently fast enough for real-time rendering, it can be used for interactive drawing applications with powerful hardware. The investigation of simplifications and optimization is an area of future work.

Our model produces acceptable results for crayons with near-solid viscosity (e.g., children's wax crayons). However, softer media, such as acrylics and pastels, would require a more complex smearing mechanism.

Refinements to our model would make it more generally applicable, both to modeling wax crayons and to related media such as acrylics. We have only marginally accounted for the orientation of the crayon itself. We could incorporate more complicated mechanics by using methods such as those of Sousa and Buchanan [SB99].

Much work still remains in simulating the predominant drawing style associated with wax crayons. Some existing work tries to model the imperfect stroke patterns that humans produce [SS02, GG01, MG02b], but we are not aware of any work on modelling the drawing styles of children.

Future work also lies in connecting our stroke primitive with a system that automatically deploys strokes. The combined system would provide a wax crayon filter, turning out crayon renditions of arbitrary 2D images, or drawings made from 3D geometry.

Acknowledgements

Thank you to Mario Sousa for his questions and comments about our work. Special thanks to Nicole Haddock, Denyse Klette, and the rest of the Belly Button BuddiesTM, as well as Cory Palmer, all for allowing us to scribble on their illustration.

References

- [Ado99] ADOBE SYSTEMS INCORPORATED: *Adobe Photoshop 5.5 Classroom in a Book*. San Jose, CA, USA, August 1999.
- [BG91] BHUSHAN B., GUPTA B. K.: *Handbook of tribology: materials, coatings, and surface treatments*. McGraw-Hill, New York, NY, USA, 1991.
- [BSLM01] BAXTER B., SCHEIB V., LIN M. C., MANOCHA D.: Dab: interactive haptic painting with 3d virtual brushes. In *Proceedings of the 28th annual conference on Computer graphics and interactive techniques* (2001), ACM Press, pp. 461–468.
- [CAS*97] CURTIS C. J., ANDERSON S. E., SEIMS J. E., FLEISCHER K. W., SALESIN D. H.: Computer-generated watercolor. In *Proceedings of the 24th annual conference on Computer graphics and interactive techniques* (1997), ACM Press/Addison-Wesley Publishing Co., pp. 421–430.
- [CJ95] CUTNEL J. D., JOHNSON K. W.: *Physics*, 3rd ed. John Wiley and Sons, Inc., New York, NY, USA, 1995.
- [Cor03] COREL CORPORATION: *Corel Painter 8 User's Guide*. Ottawa, ON, Canada, 2003.
- [GG01] GOOCH B., GOOCH A.: *Non-photorealistic rendering*. A.K. Peters, Ltd, New York, NY, USA, 2001.
- [HM92] HAASE C. S., MEYER G. W.: Modeling pigmented materials for realistic image synthesis. *ACM Transactions on Graphics (TOG)* 11, 4 (1992), 305–335.
- [JMLH01] JENSEN H. W., MARSCHNER S. R., LEVOY M., HANRAHAN P.: A practical model for sub-surface light transport. In *Proceedings of the 28th annual conference on Computer graphics and interactive techniques* (2001), ACM Press, pp. 511–518.
- [KMM*02] KALNINS R. D., MARKOSIAN L., MEIER B. J., KOWALSKI M. A., LEE J. C., DAVIDSON P. L., WEBB M., HUGHES J. F., FINKELSTEIN A.: WYSIWYG NPR: drawing strokes

- directly on 3d models. In *Proceedings of the 29th annual conference on Computer graphics and interactive techniques* (2002), ACM Press, pp. 755–762.
- [KMN*99] KOWALSKI M. A., MARKOSIAN L., NORTHROP J. D., BOURDEV L., BARZEL R., HOLDEN L. S., HUGHES J. F.: Art-based rendering of fur, grass, and trees. In *Proceedings of the 26th annual conference on Computer graphics and interactive techniques* (1999), ACM Press/Addison-Wesley Publishing Co., pp. 433–438.
- [LL94] LACROUTE P., LEVOY M.: Fast volume rendering using a shear-warp factorization of the viewing transformation. In *Proceedings of the 21st annual conference on Computer graphics and interactive techniques* (1994), ACM Press, pp. 451–458.
- [LMHB00] LAKE A., MARSHALL C., HARRIS M., BLACKSTEIN M.: Stylized rendering techniques for scalable real-time 3d animation. In *Proceedings of the first international symposium on Non-photorealistic animation and rendering* (2000), ACM Press, pp. 13–20.
- [MG02a] MAJUMDER A., GOPI M.: Hardware accelerated real time charcoal rendering. In *Proceedings of the second international symposium on Non-photorealistic animation and rendering* (2002), ACM Press, pp. 59–66.
- [MG02b] MOHR A., GLEICHER M.: HijackGL: reconstructing from streams for stylized rendering. In *Proceedings of the second international symposium on Non-photorealistic animation and rendering* (2002), ACM Press, pp. 13–ff.
- [Mou03] MOULD D.: A stained glass image filter. *Proceedings of the Eurographics Symposium on Rendering 2003* 16, 1 (June 2003), 20–25.
- [Per85] PERLIN K.: An image synthesizer. In *Proceedings of the 12th annual conference on Computer graphics and interactive techniques* (1985), ACM Press, pp. 287–296.
- [Pla95] PLASTICS DESIGN LIBRARY: *Fatigue and tribological properties of plastics and elastomers*. Norwich, NY, USA, 1995.
- [SB99] SOUSA M. C., BUCHANAN J. W.: Computer-generated graphite pencil rendering of 3D polygonal models. *Computer Graphics Forum* 18, 3 (1999).
- [SS02] STROTHOTTE T., SCHLECHTWEIG S.: *Non-photorealistic computer graphics: modelling, rendering, and animation*. Morgan Kaufmann, Natick, MA, USA, 2002.
- [TC00] TREAVENTT S. M. F., CHEN M.: Pen-and-ink rendering in volume visualisation. In *Proceedings of the conference on Visualization '00* (2000), IEEE Computer Society Press, pp. 203–210.
- [TNF99] TAKAGI S., NAKAJIMA M., FUJISHIRO I.: Volumetric modelling of colored pencil drawings. *Pacific Graphics* (October 1999).
- [VB99] VERYOVKA O., BUCHANAN J.: Halftoning with image-based dither screens. *Graphics Interface* (June 1999), 167–174.
- [VdMG91] VELHO L., DE MIRANDA GOMES J.: Digital halftoning with space filling curves. In *Proceedings of the 18th annual conference on Computer graphics and interactive techniques* (1991), ACM Press, pp. 81–90.
- [vW91] VAN WIJK J. J.: Spot noise: Texture synthesis for data visualization. *Computer Graphics (Proceedings of SIGGRAPH 91)* 25, 4 (July 1991), 309–318. ISBN 0-201-56291-X. Held in Las Vegas, Nevada.